Chemical Engineering Journal 519 (2025) 164527

Contents lists available at ScienceDirect

Chemical Engineering Journal

journal homepage: www.elsevier.com/locate/cej

CO_2 absorption kinetics and species analysis of DMEDA water-lean absorbents

Zhilv Chen [a], Chaoming Jian [b], Chao Li [a], Tao Wang [a], Qinhui Wang [a,*], Mengxiang Fang [a,*], Fanpeng Meng [b], Wei Chen [c], Yongsheng An [b], Ximing Hu [c]

[a] State Key Laboratory of Clean Energy Utilization, Zhejiang University, Hangzhou, China
[b] China Petroleum Pipeline Engineering Corporation, China
[c] Qingshanhu Energy Research Center, Zhejiang University, Hangzhou, China

ARTICLE INFO

Keywords:
CO_2 capture
Water-lean absorbent
Wetted-wall column
Mass transfer kinetics
NMR analysis
Species identification

ABSTRACT

Traditional aqueous amine-based absorbents face high energy consumption challenges in CO_2 capture processes. Replacing water with organic solvents of low viscosity, low specific heat, and high boiling point in amine-based CO_2 absorbents can effectively reduce the sensible and latent heat required for solvent regeneration. However, the introduction of organic solvents significantly alters mass transfer kinetics and chemical equilibrium, and the quantitative relationship between these effects remains unclear.

In this study, water-lean absorbents EFH series with varying organic solvent concentrations were formulated using *N*,*N*-dimethyl-1,2-ethanediamine(DMEDA), *N*,*N*-dimethylformamide (DMF), and water. Kinetic parameters were measured for DMEDA aqueous solutions, MEA aqueous solutions, pure DMF, and the EFH series. The results revealed an inconsistency between the liquid film mass transfer coefficient (k_l) and viscosity trends, indicating that physical mass transfer dominates the efficiency limitation of DMEDA absorbents under low CO_2 loading, while DMEDA retains sufficiently rapid chemical reaction rates even in water-lean environments. ^{13}C NMR analysis demonstrated that carbamate species exist as incompletely dissociated ion pairs in aprotic solvent environments. The stabilization of these ion pairs by organic solvents suppresses the generation of neutral carbamic acid, thereby restricting mass transfer and leading to an inflection point in the absorption rate. These findings highlight a dual strategy for optimizing water-lean absorbents: (1) prioritizing low-viscosity, high-CO_2-solubility solvents to enhance initial mass transfer, and (2) tuning solvent polarity or introducing proton donors to sustain reaction efficiency at higher CO_2 loadings. This work provides quantitative mechanistic insights into balancing the trade-off between chemical equilibrium and mass transfer in non-aqueous systems, offering guidance for designing energy-efficient carbon capture solvents.

1. Introduction

Amine-based absorbents are widely used in the chemical absorption of CO_2 in the flue gas. However, high energy consumption has become a significant challenge hindering their industrial application. In order to further reducing the energy consumption, optimizing solvents is an effective approach. Replacing water in amine-based absorbents with organic solvents of low viscosity, low specific heat capacity, and high boiling point to create water-lean absorbents can effectively reduce the sensible and latent heat consumed during the desorption process, thereby substantially decreasing energy consumption.

The zwitterion mechanism proposed by Caplow [1] et al. suggests that the reaction between amines and CO_2 involves formation and deprotonation of zwitterions. Since water-lean absorbents lack water as a proton transfer carrier, adopting polyamines with more active sites may be one of the effective strategies. Chen [2] et al. used *N*, *N*-dimethyl-1, 3-propanediamine (DMPA) and polyethylene glycol dimethyl (NHD) to prepare phase change water-lean absorbents. And the analysis showed that the solvent effect of NHD can decrease the energy barrier of carbamate generation from zwitterions ($DMPA^+COO^-$) to enhance chemical absorption. Jung [3] et al. developed a water-lean absorbent based on 3,3′-iminobis(*N*, *N*-dimethylpropylamine) (IBDVPA) and found that the overall mass transfer coefficient has reverse temperature dependence. Barpaga [4] designed and synthesized single-

* Corresponding authors.
E-mail addresses: qhwang@zju.edu.cn (Q. Wang), mxfang@zju.edu.cn (M. Fang).

https://doi.org/10.1016/j.cej.2025.164527
Received 11 March 2025; Received in revised form 20 May 2025; Accepted 4 June 2025
Available online 8 June 2025

component diamine water-lean absorbent N2-diisopropylethane-1,2-diamine (2-EEDIPE-DA), comprehensive evaluation showed that the formula has low viscosity and stronger affinity. Liu [5] et al. investigated the absorption performance of diethylenetriamine (DETA), triethylenetetramine (TETA) and tetraethylenepentamine (TEPA) in aqueous and n-propanol solutions. The results showed that, in addition to primary amine groups, secondary amine groups also participated in the reaction with CO_2, and the CO_2 loading increased with the number of amine groups. Moreover, the TETA/n-propanol solution could desorption at a low temperature of 363 K. In our previous work [6], we developed a series of water-lean absorbents based on the linear terminal diamine *N*, *N*-Dimethyl-1,2-ethanediamine (DMEDA) and using amides and sulfoxides as solvents. These absorbents exhibit low viscosity, high absorption and desorption rates, and high regeneration efficiency.

However, the current research on amine-based water-lean absorbents mainly focuses on the structural optimization of amines and solvents. The unique kinetics resulting from the replacement of water with organic solvents are still in the exploratory phase. Yu [7] et al. proposed that the high mass transfer coefficient of CO_2 in water-lean absorbents is attributed by the concentrated molecular and nanoscale structure of organic solvents. And the diffusion of CO_2 through pockets and channels of unreacted solvents has been observed in their representative water-lean absorbent IPADM-2-BOL. Wanderley [8] evaluated the chemical equilibrium and mass transfer rates of a series of amines such as monoethanolamine, 2-methylpiperazine, and *N*-methyldiethanolamine, as well as diluents such as sulfolane, ethylene glycol, 1-methylimidazole, dimethyl sulfoxide and *N*-methyl-2-pyrrolidone, under a fixed CO_2 partial pressure. The results indicated that, although the addition of organic solvents led to higher equilibrium partial pressures of CO_2 compared to their aqueous counterparts, the enhanced liquid film mass transfer rates resulted in faster absorption at the same partial pressures. Liu [9] et al. measured and modeled the mass transfer kinetics of 2-(ethylamino)ethanol (EAE)/*N*-methylpyrrolidone (NMP) water-lean absorbent, proposing that the high physical solubility of NMP and the high activity coefficient of EAE resulted in a faster absorption rate. Although the macroscopic properties exhibited by different absorbents are not entirely similar, numerous studies have indicated that physical solvents can enhance physical mass transfer and alter chemical equilibrium. However, the quantitative relationship between the unique kinetics and species distribution in water-lean systems is still not clear.

To quantitatively investigate species distribution in solution, ^{13}C NMR, a powerful non-invasive analytical technique, was employed in this study to investigate the forms and contents of absorption products. It has broad spectral range and there is usually no interference between peaks, providing direct qualitative and quantitative information on the components formed during the absorption or desorption of CO_2 in amine-based absorbents [10]. Although ^{13}C NMR is generally considered more suitable for qualitative research, extensive studies have confirmed that quantitative analysis of aqueous amine solutions through ^{13}C NMR is feasible [11–15]. As for water-lean systems, Lu [16] et al. employed a combined approach of ^{1}H and ^{13}C NMR to analyze the final products and reaction mechanism in the 2-amino-2-methyl-1-propanol (AMP) dual-solvent system. Kortunov [17] et al. studied a series of non-aqueous amine solutions with different basicity, including 2-ethylethylamine (EEA), aminonitrile, and piperidine. And a species quantification method for CO_2 absorption by non-aqueous amine solution through ^{1}H and ^{13}C NMR was summarized. Although the sensitivity of ^{13}C NMR is relatively poor due to low isotope abundance and slow relaxation time of the nuclear spin, it is still feasible to obtain reliable, reproducible and high-quality quantitative spectra by increasing the number of scans and relaxation time [10].

In previous work [6], we found that DMEDA water-lean absorbent and 30 wt%DMEDA aqueous solution (referred to as DMEDA(aq.)) exhibit significantly different kinetic characteristics during the absorption process: on the one hand, DMEDA water-lean absorbents can maintain much higher absorption rates than DMEDA(aq.) under low CO_2 loadings; On the other hand, the absorption rates of DMEDA water-lean absorbents sharply decrease at the inflection point as loadings increase. Yuan [18] et al. have observed similar phenomena in semi-water MEA, proposing that the depletion of MEA at the surface causes deviation from pseudo-first-order (PFO) behavior. But the causes of these phenomena are not yet fully understood. Since the organic solvent does not directly participate in the reaction, these phenomena suggest that the replacement of water with organic solvents is likely to have altered the existence form of the absorption products. To further elucidate these kinetic characteristics, we need to quantitatively describe the kinetics of DMEDA water-lean absorbents.

In addition, some studies have already revealed the species distribution of aqueous DMEDA solutions, which provides a basis for further exploring the relationship between kinetics and species distribution in water-lean systems. DMEDA, a diamine with simple structure and containing both primary and tertiary amine groups, can directly react with CO_2 to form carbamate zwitterions and also act as a proton acceptor to facilitate the deprotonation of zwitterions. A DMEDA/NMP water-lean absorbent developed by Xu [19] et al. has a relatively low viscosity (1.49 mPa·s at 313 K), high absorption and desorption rates, and excellent cyclic capacity. Yu [20,21] et al. described the reaction mechanism of the absorption of CO_2 by dilute DMEDA solution, proposing that the primary products are monoprotonated amine, monocarbamic acid, monocarbamate ions, bicarbonate/carbonate ions and very small amounts of deprotonated amine under low pH (<8). Paoletti [22] et al. assume that the products formed by protonation of primary or tertiary amine groups in asymmetric diamines such as DMEDA has a tautomeric equilibrium, which was verified by potentiometric and calorimetric methods. Therefore $^{3}NR^{1}NH^{+}$ and $^{3}NH^{+}R^{1}N$ coexist in the DMEDA solution, where the superscript x of ^{x}N represents the alkyl group substituted on N, and R represents the alkyl group. Due to the rapid intramolecular proton transfer and the stronger basicity of primary amine groups, which leads to more stable protonated products, the protonated amine can be simplified and uniformly represented as $^{3}NR^{1}NH^{+}$. So that the main reaction mechanism in DMEDA(aq.) is shown in Eqs. (1)–(3),

$$^{3}NR^{1}N + CO_2(aq) \leftrightarrow {}^{3}NR^{1}NH^{+}COO^{-} \leftrightarrow {}^{3}NR^{1}NCOOH \quad (1)$$

$$^{3}NR^{1}NH^{+}COO^{-} + {}^{3}NR^{1}N \leftrightarrow {}^{3}NR^{1}NCOO^{-} + {}^{3}NR^{1}NH^{+} \quad (2)$$

$$^{3}NR^{1}N + CO_2(aq) + H_2O \leftrightarrow {}^{3}NR^{1}NH^{+} + HCO_3^{-} \quad (3)$$

In water-lean absorbent, the mechanisms of direct reaction between primary or secondary amine groups with CO_2 are generally considered to be similar to those in aqueous solution while tertiary amine groups cannot directly react with CO_2 and only act as proton acceptors to promote deprotonation of carbamate zwitterions. These studies are of significant reference value for exploring the chemical equilibrium of DMEDA water-lean absorbents. However, due to the lack of qualitative and quantitative research on the species forms in water-lean systems, the mechanisms by which organic solvents affect physical mass transfer and chemical equilibrium remain unknown.

In this investigation, to elucidate the mechanistic effects of organic solvents on chemical equilibria and mass transfer performance, we formulated a series of water-lean EFH absorbents (DMEDA+DMF + H_2O) with varying organic solvent concentrations, alongside a benchmark 30 wt% DMEDA aqueous solution. ^{13}C NMR spectroscopy provided quantitative insights into species distribution, revealing the species transformation trends. Wetted-wall column experiments enabled precise determination of kinetic parameters, demonstrating marked contrast in absorption kinetics between aqueous and water-lean DMEDA systems. By combining both, the quantitative relationship between kinetic parameters and species distribution was investigated, thereby explaining the existence of inflection points in absorption rates observed in water-lean DMEDA absorbents.

2. Methods

2.1. Materials

The chemical information involved in the study are listed in Table 1 and Table 2.

MEA(≧99 %), DMEDA (≧98 %) and DMF(≧99.5 %) were purchased from Aladdin. CO_2 (99.999 % pure) and N_2 (99.999 % pure) gases were purchased from Hangzhou Jingong GAS *Co.*, Ltd., Hangzhou, China. Deionized water was used throughout the experiment. To simulate actual industrial application, absorbents are formulated based on mass fractions, with slight differences in molar concentrations due to different solvent densities. To simulate the water balance that needs to be maintained during actual operation, a minimum of 5 wt% water is added to the absorbent.

2.2. Experimental setup

2.2.1. Wetted-wall column (WWC)

The core principle of measuring mass transfer parameters by Wetted-wall column (WWC) is based on the dynamic interface mass transfer process between gas and liquid phases. By constructing a steady-state mass transfer interface, combining the two-film theory with Fick's laws of diffusion, this method directly correlates gas-liquid contact area, concentration gradients, and mass transfer coefficients, thereby enabling precise determination of these critical parameters. The schematic diagram is shown in Fig. 1. The WCC has a diameter d of 1.2 cm, a height h of 8.31 cm, and a gas-liquid contact area of 31.328 cm^2. The reaction chamber, solution tank, gas line, and solution line are all placed in a circulating water bath for unified temperature control, with the exposed parts undergoing thermal insulation.

A certain concentration of CO_2/N_2 mixture was prepared using mass flow controllers (SEC-E40-V, accuracy 0.5 %), preheated in the water bath, and then uniformly introduced into the reaction chamber through multiple small openings at the bottom of the apparatus. The absorbents (with a total mass of approximately 1 kg) with different CO_2 loadings were placed in the solution tank and pumped into the reaction chamber from the inside of the column through a gear pump (with a flow rate of 200 mL/min), flowing down from the top of the column to form a uniform liquid film. The gas and the liquid undergo a complete counter-current contact reaction in the reaction chamber. And then the CO_2 concentration of the gas was recorded through a CO2 infrared analyzer (GHX-3010F, accuracy 1 %). The solution after the reaction flows into the solution tank, forming a circulation. Due to the short gas-liquid contact time and large total solution mass, it can be assumed that the CO_2 loading of the solution remains constant in each experiment.

In WWC, the flux of CO_2 N_{CO2}, mol/(m^2·s), can be calculated as:

$$N_{CO2} = \frac{\delta}{A} \tag{4}$$

Where δ is the amount of CO_2 absorbed per unit time, mol/s. A is the gas-liquid contact area, m^2. Since the flow of N_2 in the intake and exhaust gas is constant, δ can be calculated as:

Table 1
Chemical information

Name	Acronym	CAS	Mol Wt	Structure
Monoethanolamine	MEA	141–43-5	61.083	
N,*N*-dimethyl-1,2-ethanediamine	DMEDA	108–00-9	88.15	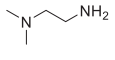
N,*N*-dimethylformamide	DMF	68–12-2	73.095	

Table 2
Absorbent formula

Absorbent	Weight			Content(mol/L)
	Amine	Solvent	H_2O	Amine
MEA(aq.)	MEA(30 wt%)	\	70 wt%	4.97
DMEDA(aq.)	DMEDA(30 wt%)	\	70 wt%	3.30
EFH5	DMEDA(30 wt%)	DMF(65 wt%)	5 wt%	3.11
EFH10	DMEDA(30 wt%)	DMF(60 wt%)	10 wt%	3.13
EFH20	DMEDA(30 wt%)	DMF(50 wt%)	20 wt%	3.16
EFH30	DMEDA(30 wt%)	DMF(40 wt%)	30 wt%	3.20

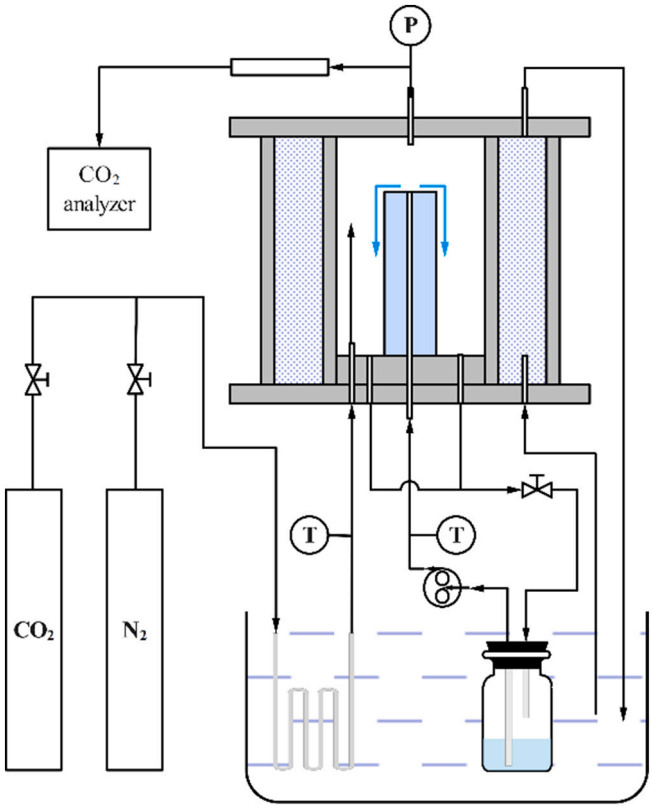

Fig. 1. The WWC device schematic.

$$\delta = \frac{Q_{in}\left(c_{CO2,in} - c_{CO2,out}\right)}{\left(1 - c_{CO2,out}\right)} \cdot \frac{P}{RT} \tag{5}$$

Where Q_{in} is the total gas volumetric flow rate, m^3/s. $c_{CO2,in}$ and $c_{CO2,out}$ are the volume fractions of the intake and exhaust gas of WWC, vol%, respectively. P and T are the pressure (Pa) and temperature (K), respectively. R is the universal gas constant, which is 8.314 J/(mol·K).

And the driving force for gas-phase mass transfer P_d, Pa, can be calculated as:

$$P_d = \frac{\left(P_{CO2,in} - P^*_{CO2}\right) - \left(P_{CO2,out} - P^*_{CO2}\right)}{\ln \frac{P_{CO2,in} - P^*_{CO2}}{P_{CO2,out} - P^*_{CO2}}} \tag{6}$$

Where $P_{CO2,in}$ and $P_{CO2,in}$ are the CO_2 partial pressure of the intake and exhaust gas of WWC, Pa. P^*_{CO2} is the corresponding CO_2 equilibrium partial pressure of the absorbent under the experimental CO_2 loading, Pa.

Since the gas-liquid contact time during the experiment is sufficiently short and the total amount of absorbent is sufficiently large, the CO_2 loading changes in a single experiment can be ignored, therefore:

$$P^{*}_{CO2} = c_{CO2,sol} H_{CO2} \quad (7)$$

Where $c_{CO2,sol}$ is the initial concentration of CO_2 in the solution, mol/m^3. H_{CO2} is the Henry's constant of CO_2, Pa·m^3/mol.

For reliability verification of the WWC, see the supplementary materials.

2.2.2. Vapor-liquid equilibrium (VLE) apparatus

The vapor-liquid equilibrium apparatus was used to measure the Henry's constants and solubilities of N_2O in the solutions, as shown in the Fig. 2. Similar methods have been widely applied and validated [23–25].

During the experiment, valves 1, 2, and 3 were opened, and the apparatus was purged with N_2 to remove residual gases. Valve 1 was then closed, and a vacuum pump was used to evacuate the buffer tank and the equilibrium chamber through gas line 4. Subsequent steps were conducted only after the temperature had stabilized at T. Valves 2 and 3 were closed, and line 4 was submerged into the solution. Valve 3 was then opened, and a certain amount of solution was drawn into the equilibrium chamber by pressure difference. The valve 3 was then closed, the mass of the solution was recorded as m and the pressure in the equilibrium chamber was recorded as P_{e1}. Valve 1 was opened to introduce a certain amount of N_2O into the buffer tank, after which valve 1 was closed. Valve 2 was opened to introduce a certain amount of N_2O into the equilibrium chamber, and then closed. The pressure in the equilibrium chamber was recorded as P_{e2}. After the temperature and pressure stabilized, indicating the attainment of gas-liquid equilibrium, the pressure in the equilibrium chamber decreased due to the dissolution of N_2O, recorded as P_{e3}.

The Henry's constants and solubilities of N_2O in the solutions can be calculated by the following equation:

$$H_{N2O,l} = P_{e3} / c_{N2O} \quad (8)$$

$$c_{N2O} = \frac{(P_{e2} - P_{e1} - P_{e3})\left(V_e - \frac{m}{\rho}\right)\cdot\rho}{RTm} \quad (9)$$

Where c_{N2O} is the solubility of N_2O in the solution, mol/m^3 ; ρ is the density of the solution, kg/m^3.

2.2.3. ^{13}C Nuclear Magnetic Resonance (^{13}C NMR)

In this study, an Agilent DD2 600 MHz nuclear magnetic resonance instrument was used to perform ^{13}C NMR species identification. An 11 wt% solution of 1,4-dioxane in deuterated water was used as an internal standard. It was employed for both signal locking and chemical shift calibration. The internal standard was encapsulated in a capillary tube and then placed inside the NMR tube to prevent mixing with the sample and altering the chemical reaction equilibrium [12–14]. The parameters used in the experiment: delay time, D1 = 60 s (≥5 T1), number of scans, NS = 300. Data processing was performed using MestReNova software. The NMR acquisition was performed with a scan number (NS) set to 300 and a relaxation delay (D1) of 60 s.

The software Mestrenova was used to process the data.

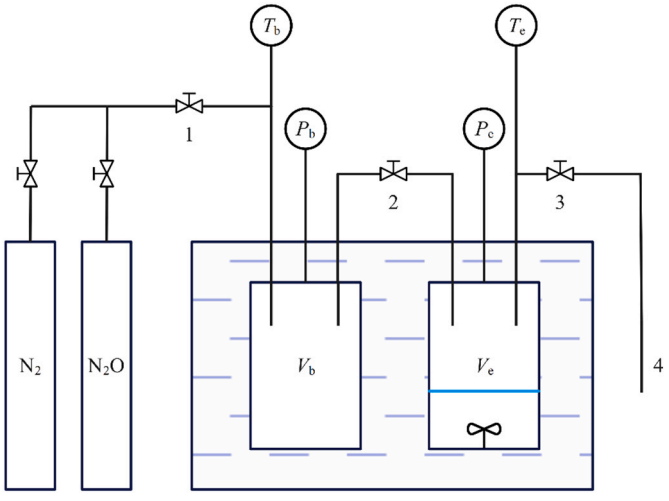

Fig. 2. The vapor-liquid equilibria (VLE) apparatus schematic.

2.3. Mass transfer kinetics

2.3.1. Overall mass transfer coefficient K_G

According to the film theory of mass transfer, the mass transfer resistance across the gas-liquid interface can be expressed as:

$$\frac{1}{K_G} = \frac{1}{k_g} + \frac{1}{k_l} \quad (10)$$

Where K_G is the overall mass transfer coefficient. k_g and k_l are the gas film and liquid film mass transfer coefficients. In the mass transfer experiment of WWC, the overall mass transfer coefficient K_G can be calculated as:

$$K_G = \frac{N_{CO2}}{P_d} \quad (11)$$

2.3.2. Gas film mass transfer coefficient k_g

The empirical model provided by Pacheco [26] et al. points out that the gas film mass coefficient k_g can be calculated by the Sherwood number, and this model has been widely used in calculating k_g in WWC. As shown below:

$$k_g = \frac{Sh \cdot D_{CO2,g}}{RTd} \quad (12)$$

$$Sh = 1.075 \cdot \left(\frac{Re \cdot Sc \cdot d}{h}\right)^{0.85} = 1.075 \cdot \left(\frac{v_g d^2}{D_{CO2,g} h}\right)^{0.85} \quad (13)$$

$$Re = \frac{\rho_g v_g d}{\mu_g} \quad (14)$$

$$Sc = \frac{\mu_g}{\rho_g D_{CO2,g}} \quad (15)$$

Where Sh, Re and Sc are Sherwood number, Reynolds number, and Schmidt number, respectively. $D_{CO2,g}$ is the diffusion coefficient of CO_2 in the gas phase, m^2/s, calculated by the methods proposed by Fuller [27] et al. d and h are the hydraulic diameter and height of the WCC, m. $\rho_g$is the density of the gas phase, kg/m^3. v_g is the flow velocity of the gas, m/s. μ_g is the dynamic viscosity of the gas phase, Pa·s。

2.3.3. Liquid film mass transfer coefficient k_l

When mass transfer is accompanied by a chemical reaction, the liquid film mass transfer coefficient k_l can be expressed as:

$$k_l = \frac{E k_l^0}{H_{CO2}} \quad (16)$$

Where E is the chemical reaction enhancement factor. k_l^0 is the liquid film physical mass transfer coefficient, m/s.

According to the optimization model of liquid physical mass transfer coefficient proposed by Pacheco [26] et al., k_l^0 can be calculated by the following formula in this study:

$$k_l^0 = \frac{3Q_l}{A}\sqrt{\frac{\varepsilon}{\pi}} \quad (17)$$

$$\varepsilon = \frac{D_{CO2,l}h}{v_l\delta^2} \tag{18}$$

Where Q_l is the liquid volumetric flow rate, m^3/h. A is the gas-liquid contact area, m^2. ε is a dimensionless number. $D_{CO2,l}$ is the diffusion coefficient of CO_2 in the liquid phase, m^2/s. v_l is the flow velocity of the liquid, m/s. δ is the thickness of the liquid film, m. Where v_l and δ can be calculated as:

$$v_l = \frac{\rho_l g\delta^2}{2\mu_l} \tag{19}$$

$$\delta = \sqrt[3]{\frac{3\mu_l Q_l}{\rho_l gL}} \tag{20}$$

Where ρ_l is the density of the liquid phase, kg/m^3. g is the gravity acceleration, 9.8 m/s^2. μ_l is the dynamic viscosity of the liquid phase, Pa·s ; L is the circumference of the WWC, m.

2.3.4. Chemical reaction enhancement factor *E*

The chemical reaction enhancement factor E is a dimensionless parameter that quantifies the intensification of mass transfer rate due to chemical reaction. This phenomenon originates from the removal of solutes at the gas-liquid interface through reactive consumption, which sustains the driving force for mass transfer. In the fast pseudo-first-order reaction regime, E is related to the Hatta number Ha and the infinite enhancement factor E_∞:

$$Ha = \frac{\sqrt{k_{ov}D_{CO2,l}}}{k_l^0} \tag{21}$$

$$E_\infty = \sqrt{\frac{D_{CO2,l}}{D_{prod}}}\left(1 + \frac{D_{prod}}{D_{CO2,l}}\frac{H_{CO2}c_{prod}}{v_{prod}P_{CO2}}\right) \tag{22}$$

Where k_{ov} is the overall kinetic constant, s^{-1}. D_{prod} is the diffusion coefficient of the product, m^2·s. c_{prod} is the concentration of the product, mol/L. v_{prod} is the stoichiometric coefficient of the reaction product. When $3<Ha<E_\infty$, the E can be considered equal to the Ha [28], that is:

$$E = \frac{A}{3Q_l}\sqrt{\frac{k_{ov}v_l\delta^2}{h}} \tag{23}$$

2.3.5. Diffusion coefficient

The diffusion coefficient of CO_2 in amine solution is correlated with the diffusion coefficient in water [29], as shown below:

$$D_{CO2,l} = D_{CO2,H2O}\cdot\left(\frac{\mu_{H2O}}{\mu_l}\right)^{0.8}(m^2\cdot s) \tag{24}$$

$$D_{CO2,H2O} = 2.35\times10^{-6}\exp\left(-\frac{2119}{T}\right)(m^2\cdot s) \tag{25}$$

The viscosity of water at different temperatures is calculated by empirical formula [30]:

$$\mu_{H2O} = \frac{(T-273.15)+246}{55.94(T-273.15)^2+5284.2(T-273.15)+137370}(Pa\cdot s) \tag{26}$$

2.3.6. Henry's constant

Since the chemical reaction between CO_2 and amine interferes with the measurement of physical solubility, the N_2O analogy method is usually used to estimate the Henry's constant of CO_2 [29], as shown below:

$$H_{CO2,l} = H_{N2O,l}\left(\frac{H_{CO2,H2O}}{H_{N2O,H2O}}\right) \tag{27}$$

$$H_{N2O,H2O} = 8.55\times10^6\exp\left(-\frac{2284}{T}\right) \tag{28}$$

$$H_{CO2,H2O} = 2.82\times10^6\exp\left(-\frac{2044}{T}\right) \tag{29}$$

Where $H_{N2O,l}$, $H_{CO2,l}$, $H_{N2O,H2O}$ and $H_{CO2,H2O}$ are the Henry's constant of N_2O and CO_2 in amine solution and water, respectively, $Pa\cdot m^3\cdot mol^{-1}$. Among them, $H_{N2O,l}$ can be obtained through VLE experiments.

3. Results and discussion

3.1. Species identification and reaction mechanism

3.1.1. Species inference and reaction pathways

^{13}C NMR analysis was performed on DMEDA(aq.) and EFH under different CO_2 loadings. And the main species in the solution were inferred based on peak area and chemical shift. The structure formulas and reaction pathways are shown in Fig. 3.

The ^{13}C NMR spectrum of DMEDA (aq.) is shown in Fig. 4. It can be observed that under low CO_2 loading, the reaction products are mainly composed of $^3NR^1NCOO^-$/$^3NR^1NCOOH$ (164.23–164.01 ppm). Due to the rapid proton exchange in the aqueous solution, the two exhibit an identical narrow peak C_d. When the loading reaches 0.47 mol/mol, a characteristic peak C_e of compounds HCO_3^- and CO_3^{2-} appears at 163.16 ppm. As the reaction progresses, the peak area gradually increases and the chemical shift moves upfield to 160.41 ppm. This is attributed to the increase in the ratio of HCO_3^-/CO_3^{2-} as the pH decreases. For the α-C of DMEDA molecules, all characteristic peaks split upon the formation of carbamates, resulting in the appearance of additional peaks (C_a' , C_b'和 C_c'). Additionally, DMEDA molecule acts as proton acceptor, facilitating the deprotonation of the carbamate zwitterion. The protonation product are $^3NR^1NH^+$ and $^3NH^+R^1N$, which exist in tautomeric equilibrium [22]. As the degree of protonation increases, α-C shifts significantly upfield, but no splitting occurs (C_a, C_b and C_c).

The water-lean systems exhibit comparable product compositions, with EFH5 presented as a representative example (see Supplementary Materials for full spectral data). As shown in the Fig. 5, the NMR spectrum of fresh EFH5 is split due to the spin coupling of protons, but quantitative analysis can be performed by the sum of the areas of the split peaks. C_f , C_g are the solvent peaks (the solvent peak C_h at 30 ppm is cut off), and no splitting or obvious shift occurs, which indicates that DMF essentially does not participate in the reaction. The carbonyl peak C_d* of the by-product was observed in the range of 161.83–162.15 ppm, which is different from DMEDA (aq.). Kortunov [17] et al. have pointed out that in non-aqueous solvent with high amine concentration and high alkalinity (high pKa), the carbamic acid and free amine can undergo dehydration to form urea. However, under all loadings, C_d*:C_b*:C_a*:C_c* ≈ 1:1:2:1, which means that the chemometric ratio of CO_2 and DMEDA in the side reaction is 1:1, rather than 1:2 of urea formation. Therefore, the product is likely to be an anhydride formed by carbamic acid dehydration, as shown in Fig. 3.The remaining characteristic peaks of EFH5 are similar to those of DMEDA(aq.), shift upfield and split as the loading increases, but with more pronounced broadening. This is due to the reduced intermolecular transfer rate of protons, resulting from the lack of water as a proton transfer carrier. As can be seen in Fig. 5, only C_c split at the beginning of the reaction, which may be resulted from partial dissociation of the carbamate ion pairs.

3.1.2. Quantitative analysis of species transformation

The rapid transfer of protons can lead to indistinguishable species, which means that the species in amine solution cannot be precisely quantified solely through ^{13}C NMR. However, based on mass conservation, charge balance and chemical shift, it is possible to analyze the species transformation corresponding to the NMR spectrum. The

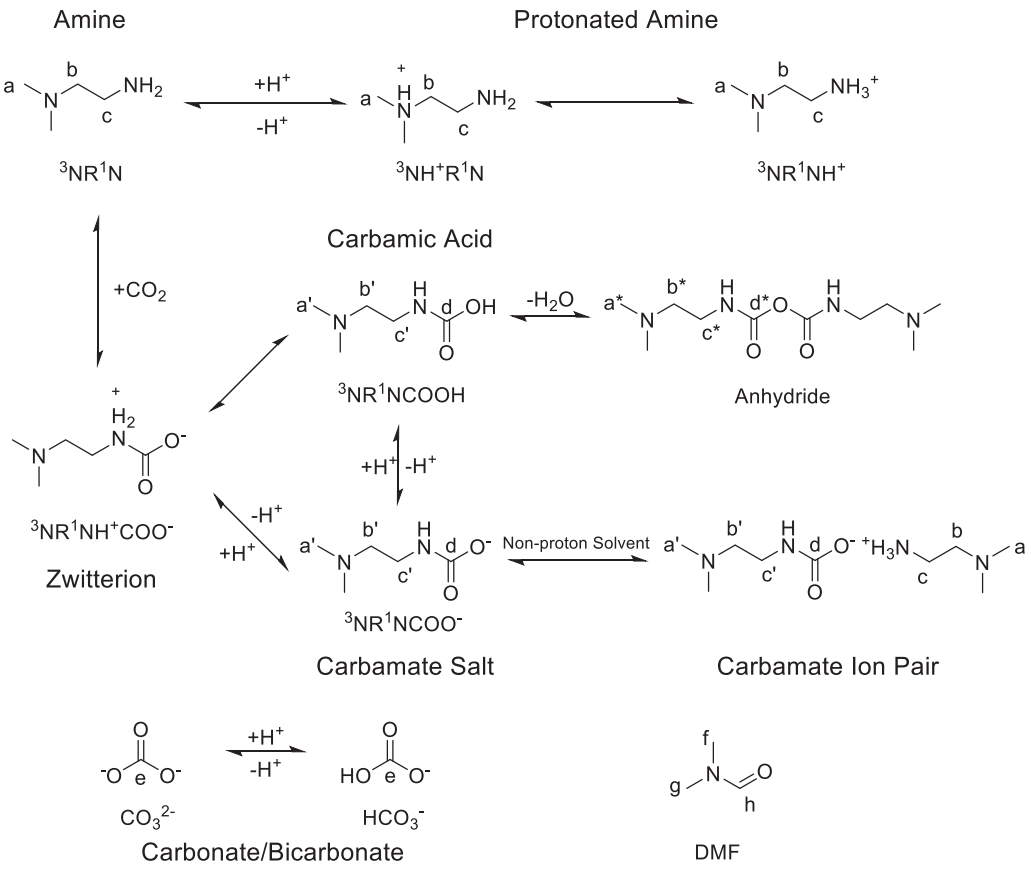

Fig. 3. The structure formulas and reaction pathways.

quantitative calculation of species in this study referenced some methods from Kortunov [17] et al. For species such as DMEDA/DMEDAH+ that are difficult to distinguish, their concentrations were estimated based on the chemical shift offsets. The concentrations of the remaining species were calculated based on mass conservation and charge balance. Detailed data and estimation methods are provided in the Supplementary Materials. The transformation trends of the main species in DMEDA(aq.) and EFH series were shown in Fig. 6.

The transformation trends of main species in DMEDA(aq.) are consistent with the literature [20]. At the beginning of the reaction, the concentration of carbamate is slightly higher than that of neutral carbamic acid, but the proportion of carbamic acid exceeds carbamate when the loading increases to about 0.25 mol/mol, becoming the main product. For carbamate, the concentration gradually increases until the loading reaches 0.59 mol/mol, and then the degree of hydrolysis increases and gradually transforms into carbamic acid. Finally, when the loading reaches 0.95 mol/mol, carbamic acid can account for 87 % of the total loading. In addition, when the loading reaches 0.47 mol/mol, a small amount of HCO_3^-/CO_3^{2-} can be detected in the solution, and the concentration gradually increases as the loading increases. Since the CO_3^{2-} content is quite low, the subsequent discussion only focus on the concentration of HCO_3^-. Upon reaching a loading of 0.80 mol/mol, the concentration of free amine becomes insufficient, causing water to react directly with CO_2. Consequently, the concentration of HCO_3^- increases significantly, eventually comprising 11 % of the total loading.

For EFH5, since the high concentration of amine and high alkalinity, carbamate is rapidly generated in large quantities under low CO_2 loading, while only a small amount of carbamic acid is generated, which is consistent with the literature [17]. Additionally, in the water-lean environment with high pH, a portion of carbamic acid undergoes dehydration to form the anhydride by-product. However, the by-product does not continue to accumulate with increasing loading. Instead, after the loading reaches 0.3 mol/mol, it gradually transforms into other forms as the pH decreases. When the loading reaches 0.48 mol/mol, the concentration of free amine is as low as 0.63 mol/L. The deprotonation process of carbamate zwitterion lacks proton acceptors, making it more prone to undergo internal proton transfer to form carbamic acid. At the same time, protonated amine further participates in the reaction, causing the carbamate to receive proton to form neutral acid. Around a loading of 0.54 mol/mol, the concentration of carbamic acid exceeds carbamate, becoming the dominant species. And under the final loading of 0.85 mol/mol, carbamic acid accounts for 78 % of the total loading. Due to the lack of water, only a very small amount of bicarbonate product exists even when the solution tends to be saturated, which ultimately accounts for 4.2 % of the total products.

The EFH series demonstrates similar species distributions with distinct transformation patterns. In EFH10 at 0.58 mol/mol, a sharp increase in carbamate concentration can still be observed, whereas no distinct inflection point is discernible in EFH20, indicating that the solution properties approach those of the aqueous solution. The slight increase in bicarbonate content with higher water content further demonstrates this trend. As organic solvent concentration reduces, carbamate acid predominance escalates in final product. In EFH30, it reaches 90.6 % of the product composition, which is higher than that in DMEDA(aq.). This shows that carbamate content does not follow a simple trend with the concentration of organic solvent. Furthermore, the reduced organic solvent concentration destabilizes the carbamate ion pairs, causing the by-product anhydride content to initially increase slightly but subsequently decrease gradually due to hydrolysis reactions.

3.2. Correlation between viscosity and kinetics

The diffusion coefficient of CO_2 in the liquid phase is closely related to the viscosity, while changes in temperature and CO_2 loading will lead

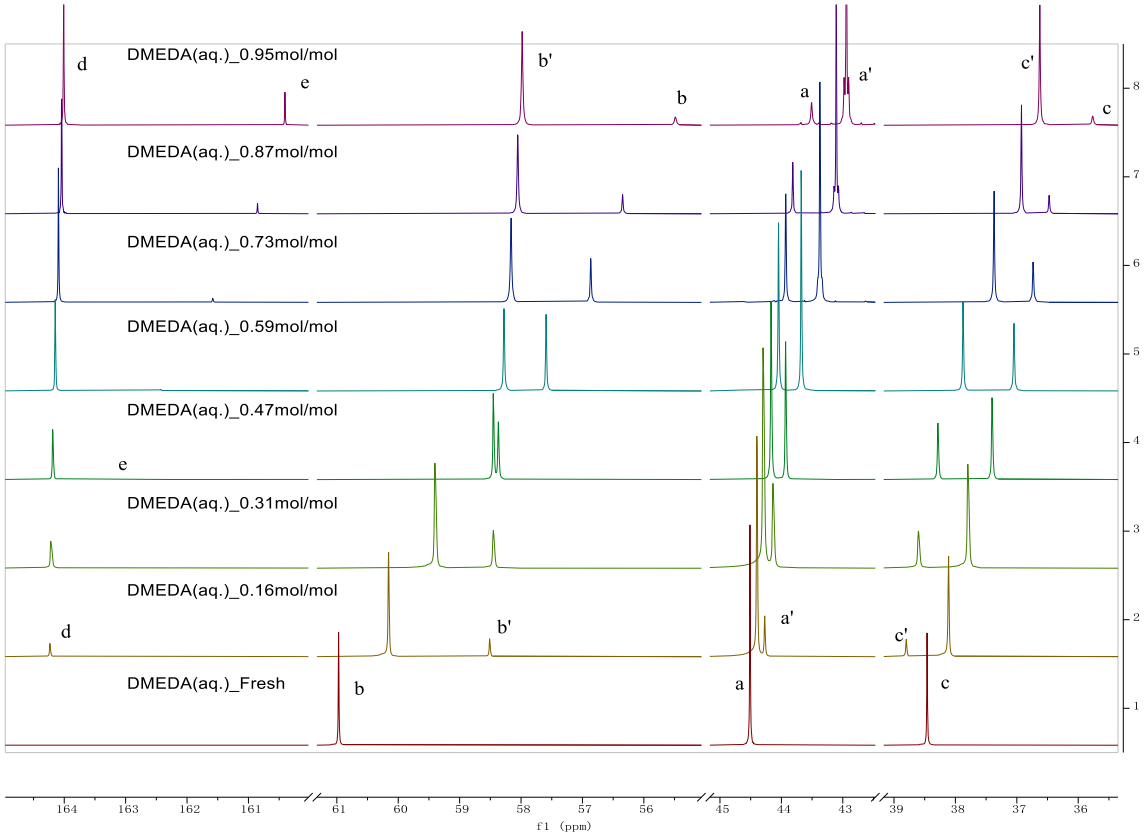

Fig. 4. The ^{13}C NMR spectrum of DMEDA (aq.)

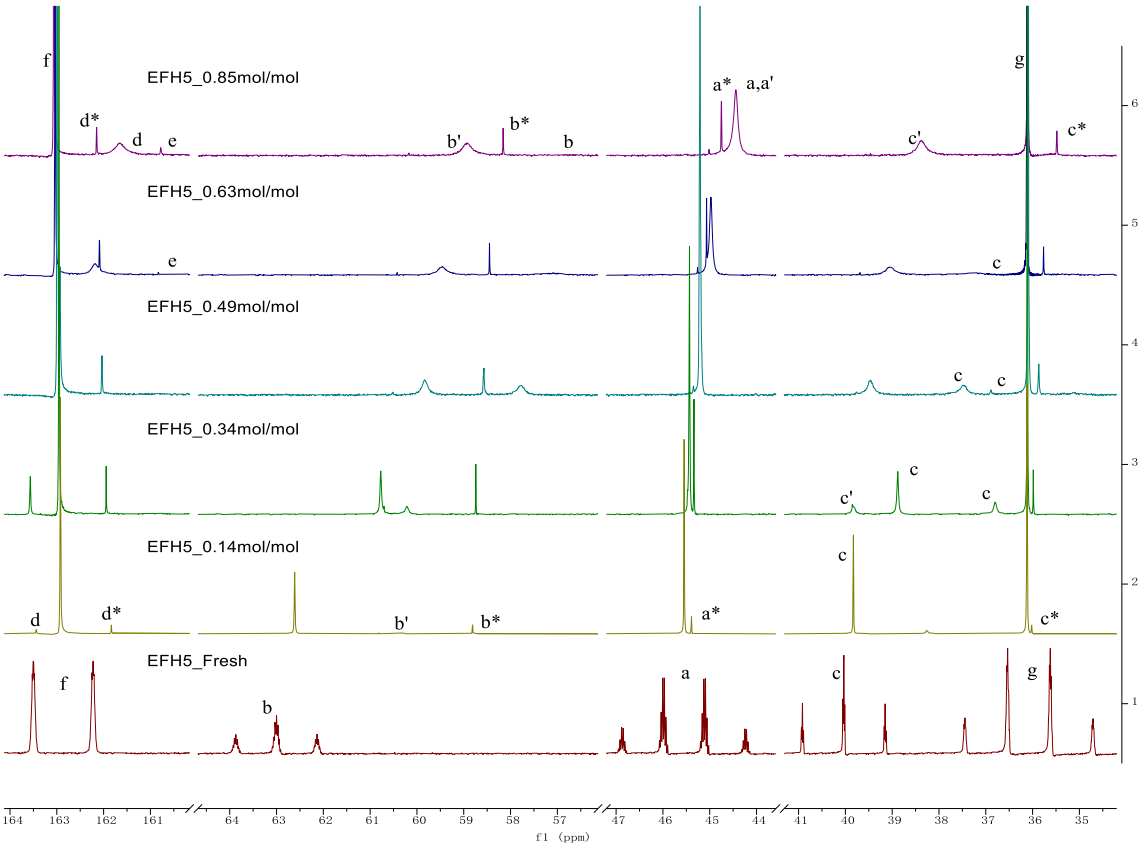

Fig. 5. The ^{13}C NMR spectrum of EFH5.

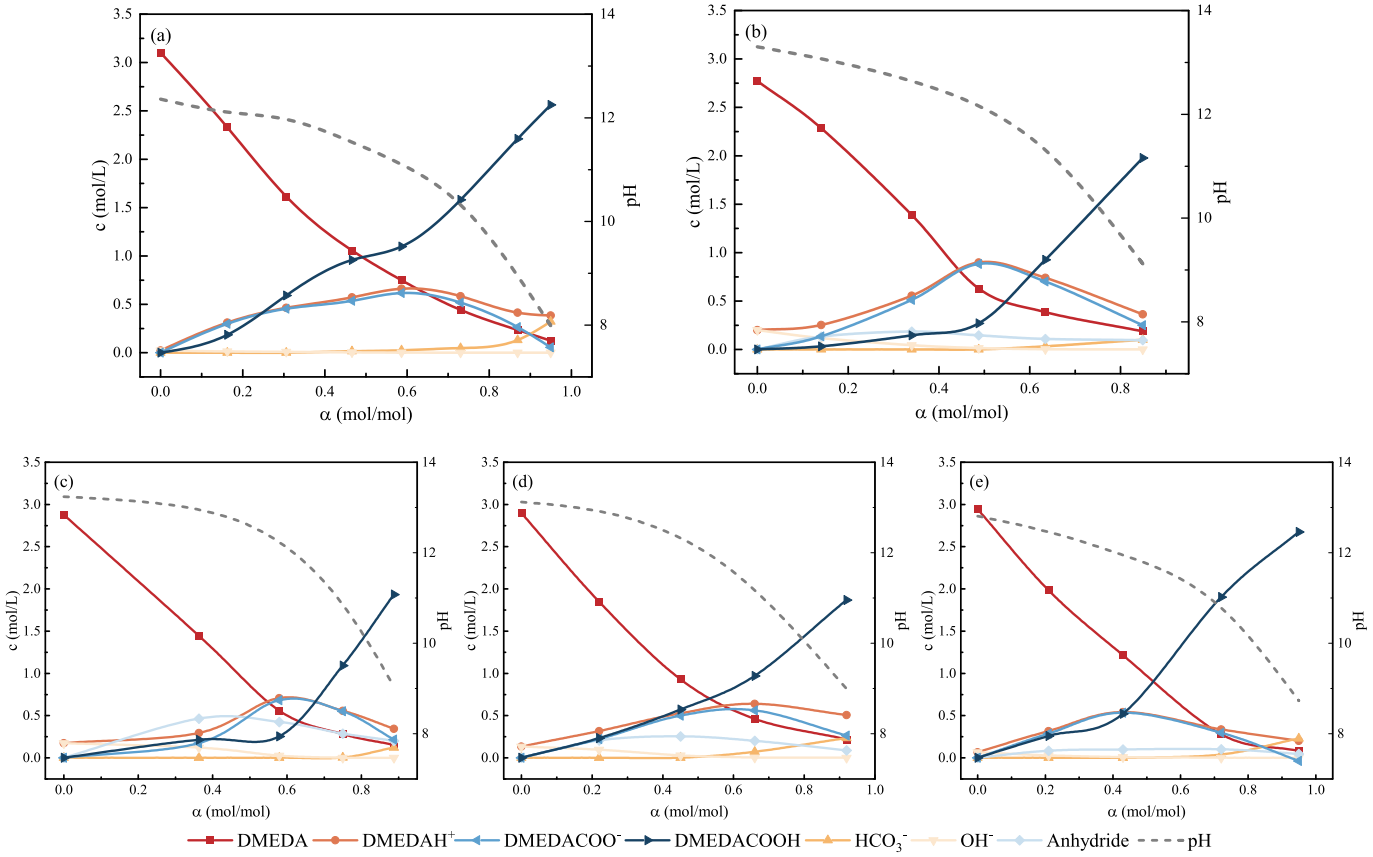

Fig. 6. The transformation trends of the main species in (a) DMEDA(aq.), (b) EFH5, (c) EFH10, (d) EFH20 and (e) EFH30.

to changes in solution viscosity. The viscosities of MEA(aq.), DMEDA (aq.), DMF and EFH series were measured using a digital rotational viscometer(DV-II + Pro, accuracy of 1 %) at various temperatures and under different CO_2 loadings, as shown in Fig. 7. Within the temperature range of 303.15 K to 333.15 K, the viscosities of the liquids are ranked from highest to lowest as DMEDA(aq.) > MEA(aq.) > EFH5 > DMF. As the temperature increases, the viscosities of all four liquids decrease. Among them, the viscosity of DMEDA(aq.) decreases the most, with a reduction of 67.2 %. The viscosities of liquids MEA(aq.), EFH5 and DMF decrease by 43.8 %, 42.8 %, and 24.3 %, respectively.

For the EFH series, the viscosity increases with higher water content, reaching levels comparable to MEA(aq.) when water content attains 10 wt%. Additionally, the viscosity decline trend of the EFH series progressively approaches that of DMEDA(aq.) with increasing water content, where EFH30 exhibits a 53.8 % viscosity reduction during a temperature rise of 30 °C. However, within this temperature range, EFH30 consistently maintains higher viscosity than EFH5, demonstrating that maintaining lower water content helps preserve the mass

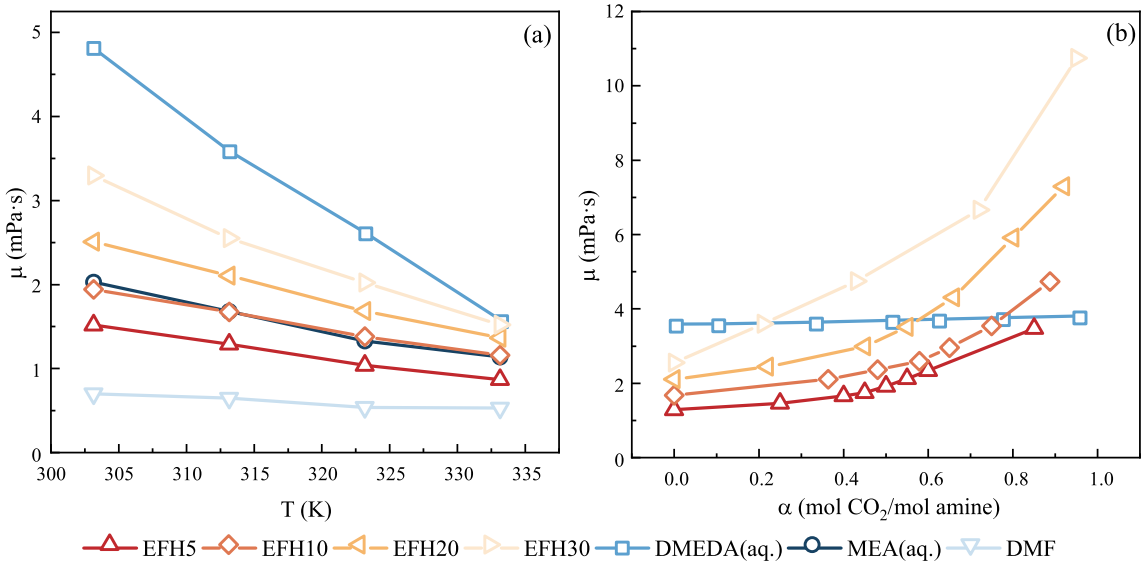

Fig. 7. The viscosity changes with temperature and CO_2 loading.

transfer performance advantages of EFH water-lean absorbents.

During the CO_2 absorption of, the viscosity increase trend of DMEDA (aq.) is flat, with only 6.1 %. In contrast, the EFH series demonstrates gradual viscosity growth under low CO_2 loadings, followed by accelerated escalation beyond threshold loading levels. Taking EFH5 as an example, the viscosity shows a significant increase trend after the loading reaches approximately 0.45 mol/mol, and eventually increases by 169.0 %. This trend closely parallels the rising carbamate content profile observed in EFH5. With water content increasing to 30 wt%, the EFH series shows a more significant viscosity increase. The viscosity of EFH30 ultimately rises by 321.2 %, and its saturate capacity is significantly higher than that of DMEDA(aq.). This phenomenon further reveals that neutral carbamates abundantly generated during the mid-absorption phase in EFH series exhibit intensified intermolecular interactions. Their hydrogen-bonding networks with polar solvents alter solution microstructure, thereby driving substantial viscosity enhancement.

3.3. Effect of temperature on kinetics

The kinetic parameters of MEA(aq.), DMEDA(aq.), DMF and EFH series were measured within the temperature range of 303.15 K to 333.15 K. The liquid film mass transfer coefficient k_l was shown in Fig. 8. Other parameters such as gas film mass transfer coefficient k_g, Henry's constant H and chemical reaction enhancement factor E, etc. are shown in Table 2.

Although the k_l of DMEDA(aq.) is lower than that of MEA(aq.) , EFH5 with the same main agent DMEDA has a significantly higher k_l. However, it can be observed from Table 3 that at 313.15 K, the chemical reaction enhancement factor E of EFH5 is only 58.7 % of that of DMEDA (aq.). This is because, the lack of proton carriers hinders the deprotonation of carbamate zwitterionic ions in water-lean solution. This also implies that the mass transfer performance of DMEDA (aq.) is primarily limited by the physical mass transfer rate rather than the chemical reaction rate. The addition of DMF reduced the viscosity of the system, increased the liquid-phase diffusion coefficient and solubility of CO_2, thereby significantly enhancing the liquid film mass transfer coefficient. However, despite the lower viscosity and higher physical solubility, the pure DMF exhibits a much lower k_l, being only 2.8 % of that of EFH5. This suggests that the strong mass transfer performance of the amine-based water-lean absorbent is not only due to the enhancement of physical mass transfer process by the organic solvent. Furthermore, the

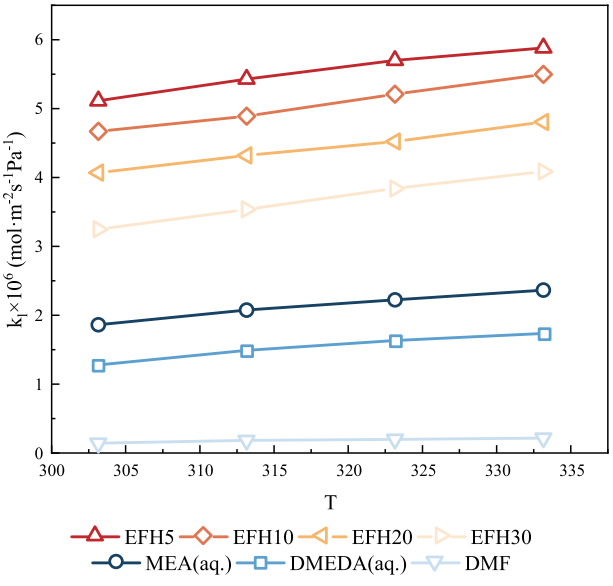

Fig. 8. Temperature dependence of liquid film mass transfer coefficient(k_l).

E of EFH20 and EFH30 surpass that of DMEDA(aq.), confirming that DMEDA retains sufficiently fast reaction kinetics even in water-lean systems where proton carriers are limited.

It is also worth noting that, although the temperature increase limits the physical dissolution of CO_2, due to the decrease in the viscosity, the increase in the diffusion coefficient, and the increase in the chemical reaction rate, the k_l of the liquids increases as temperature increases in the range of 303.15 K to 333.15 K. However, the increase gradually diminishes as the temperature rises. For the two aqueous amine solutions MEA(aq.) and DMEDA(aq.), the k_l increased by 5.0×10^{-7} mol·m^{-2}·s^{-1}·Pa^{-1}(27.4 %) and 4.5×10^{-7} mol·m^{-2}·s^{-1}·Pa^{-1}(36.0 %), respectively, with a similar magnitudes of increase. This is attributed to the similar chemical reaction mechanisms of the aqueous amine solutions. However, the liquid film mass transfer of DMEDA(aq.) is relatively more constrained by its higher viscosity. As the temperature rises, its viscosity decreases significantly, resulting in a relatively larger increase in k_l. For the EFH series, take EFH5 as an example, the k_l increased by 7.7×10^{-7} mol·m^{-2}·s^{-1}·Pa^{-1} from 303.15 K to 333.15 K, with the absolute increase of 1.7 times that of DMEDA (aq.) and 10.4 times that of DMF, despite the viscosity reduction is not as obvious as that of DMEDA (aq.). As can be seen from Table 2, the chemical enhancement factor E of EFH increased by 54.8 %, higher than 31.1 % of DMEDA (aq.), which shows that temperature increase within a certain range has a more significant enhancement effect on the chemical reaction of EFH to absorb CO_2. And it also revealed that there are differences in the reaction mechanism of EFH and DMEDA(aq.) to absorb CO_2.

3.4. Effect of CO_2 loading on kinetics

The kinetic parameters of DMEDA(aq.) and EFH series under different CO_2 loadings at 313.15 K were measured, k_l was shown in Fig. 9. CO_2 loading dependence of liquid film mass transfer coefficient (k_l), and other parameters were shown in Table 4.

The variation of k_l reveals significant differences in the mass transfer kinetics of EFH5 and DMEDA(aq.). The k_l of the fresh EFH5 can reach 3.6 times that of DMEDA (aq.). As the CO_2 loading increases, the k_l of both decreases. But it is worth noting that before the loading reaches about 0.56 mol/mol, the k_l of EFH5 is higher than that of DMEDA(aq.). This shows a broader operating range for EFH5 compared to DMEDA (aq.), consistent with our previous bubble absorption tests.

In addition, the k_l of EFH5 shows a sharp decrease between 0.40 and 0.55 mol/mol. The decrease in k_l within this range accounts for 63.5 % of the total decrease, although the viscosity increase within this range was only 21.1 % of the total increase(Fig. 3). This means that the reduction of the k_l is not only attributed to the physical mass transfer limitation caused by the increase in viscosity, but also to the change in the rate-determining step of the reaction, which is likely caused by the substantial consumption of free amine. The 82.9 % decrease in E shown in Table 3 also reflects this point.

EFH10 demonstrates a k_l comparable to EFH5, showing an abrupt decline within the 0.48–0.65 mol/mol loading range. However, with reduced organic solvent concentration, EFH20 and EFH30 exhibit significantly lower initial k_l values, and no distinct inflection points emerge with increasing loading. While physical mass transfer advantages gradually weaken, EFH30 containing the minimal organic solvent concentration still exhibits superior mass transfer performance compared to DMEDA(aq.) until 0.7 mol/mol loading. This reveals that proton transfer no longer governs chemical reaction kinetics at this water content level. Instead, the stabilizing effect of organic solvents on carbamate ion pairs promotes the deprotonation of carbamate zwitterions.

3.5. Mass transfer kinetics of absorption process

In the early stages of the absorption reaction, the reaction paths of EFH series and DMEDA (aq.) are similar. Due to the strong basicity of

Table 3
CO_2 absorption kinetics parameters at different temperatures

	T	K_G*	k_g*	k_l*	k_l^0	μ_l	ρ_l	$D_{CO2,l}$	$H_{CO2,l}$	E*
	K		mol·m^{-2}·s^{-1}·Pa^{-1}		m/s	mPa·s	kg/m^3	m^2/s	Pa·m^3·mol^{-1}	
MEA(aq.)	303.15	1.76E-06	3.28E-05	1.86E-06	7.90E-05	2.03	1009.0	1.02E-09	3436	80.9
	313.15	1.95E-06	3.27E-05	2.07E-06	9.07E-05	1.68	1003.0	1.27E-09	4175	95.5
	323.15	2.08E-06	3.14E-05	2.22E-06	1.07E-04	1.33	998.1	1.64E-09	5080	106
	333.15	2.20E-06	3.09E-05	2.36E-06	1.21E-04	1.14	993.5	1.99E-09	6194	121
DMEDA (aq.)	303.15	1.23E-06	3.27E-05	1.28E-06	4.81E-05	4.81	967.4	5.14E-10	2931	77.8
	313.15	1.42E-06	3.21E-05	1.49E-06	5.86E-05	3.59	961.2	6.92E-10	3717	94.4
	323.15	1.55E-06	3.12E-05	1.63E-06	7.23E-05	2.62	954.7	9.52E-10	4310	97.2
	333.15	1.64E-06	3.05E-05	1.73E-06	9.97E-05	1.58	947.1	1.53E-09	5850	102
DMF	303.15	3.06E-05	1.42E-07	1.43E-04	\	0.70	940.3	2.40E-09	540.8	
	313.15	3.00E-05	1.83E-07	1.54E-04		0.65	934.2	2.71E-09	654.6	\
	323.15	2.93E-05	1.99E-07	1.76E-04	\	0.54	926.8	3.37E-09	803.0	
	333.15	2.85E-05	2.16E-07	1.84E-04		0.53	916.5	3.67E-09	973.5	\
EFH5	303.15	4.41E-06	3.29E-05	5.09E-06	9.17E-05	1.52	920.5	1.29E-09	884.4	49.1
	313.15	4.63E-06	3.22E-05	5.41E-06	1.04E-04	1.29	914.7	1.57E-09	1063	55.4
	323.15	4.81E-06	3.15E-05	5.68E-06	1.21E-04	1.04	905.4	1.99E-09	1380	64.7
	333.15	4.92E-06	3.09E-05	5.86E-06	1.38E-04	0.87	895.0	2.47E-09	1798	76.0
EFH10	303.15	4.09E-06	3.26E-05	4.67E-06	7.98E-05	1.94	925.4	1.06E-09	1017	59.5
	313.15	4.24E-06	3.18E-05	4.89E-06	8.96E-05	1.68	920.1	1.27E-09	1238	67.6
	323.15	4.47E-06	3.12E-05	5.21E-06	1.03E-04	1.38	910.2	1.59E-09	1570	79.2
	333.15	4.66E-06	3.07E-05	5.50E-06	1.18E-04	1.16	901.3	1.96E-09	2094	97.7
EFH20	303.15	3.62E-06	3.27E-05	4.07E-06	6.92E-05	2.51	935.4	8.65E-10	1328	78.1
	313.15	3.81E-06	3.23E-05	4.32E-06	7.88E-05	2.11	929.1	1.06E-09	1637	89.8
	323.15	3.95E-06	3.14E-05	4.52E-06	9.24E-05	1.69	923.3	1.36E-09	2052	100
	333.15	4.15E-06	3.04E-05	4.81E-06	1.07E-04	1.37	912.9	1.72E-09	2666	119
EFH30	303.15	2.96E-06	3.29E-05	3.25E-06	5.94E-05	3.30	944.3	6.95E-10	1635	89.4
	313.15	3.19E-06	3.21E-05	3.54E-06	7.08E-05	2.55	939.5	9.10E-10	2062	103
	323.15	3.42E-06	3.11E-05	3.84E-06	8.33E-05	2.02	926.5	1.17E-09	2428	112
	333.15	3.60E-06	3.04E-05	4.08E-06	1.01E-04	1.52	917	1.58E-09	3221	130

* The values in this column are the arithmetic means of measurements taken at four different CO_2 partial pressures.

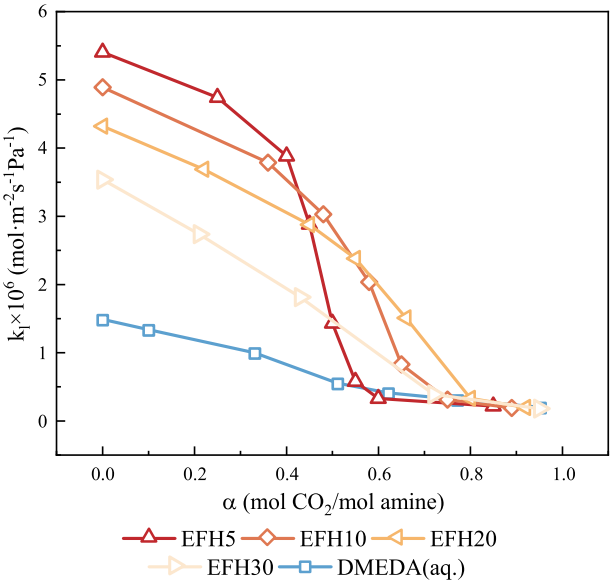

Fig. 9. CO_2 loading dependence of liquid film mass transfer coefficient(k_l)

primary amine group, carbamate zwitterion tends to convert to carbamate. This process is extremely rapid, so the mass transfer performance of the liquid film at the beginning of the reaction depends on the physical mass transfer performance. EFH series have an advantage with its low viscosity, high CO_2 diffusion coefficient and CO_2 solubility. Subsequently, since the carbamate is easily hydrolyzed in aqueous solution to form carbamic acid, and can exist relatively stable in the form of ion pairs in aprotic polar solvent, the neutral acid content in DMEDA (aq.) is significantly higher than that in EFH series.

As the reaction proceeds, the deprotonation of carbamate zwitterion is impeded, and the neutral carbamic acid formed via intramolecular proton transfer gradually becomes the dominant product. Meanwhile, the concentration of free amine decreases, prompting carbamate to further participate in the reaction. This step of the reaction is relatively slow. However, the liquid film mass transfer performance of DMEDA (aq.) is consistently dominated by physical mass transfer properties, and water, acting as a proton carrier, facilitates the deprotonation of protonated amine, resulting in a relatively gradual decrease in k_l. In contrast, the proton transfer of carbamate ion pairs in EFH series becomes a key step in reaction kinetics, as shown in Fig. 10. Proton transfer of carbamate ion pairs. Due to the stabilizing effect of organic solvents on carbamate ion pairs, the k_l of EFH5 and EFH10 decreases sharply. In contrast, EFH20 and EFH30, with their relatively higher water content, undergo hydrolysis of the carbamate, resulting in an increase in carbamic acid content under lower loadings. In addition, the large amount of carbamic acids generated at this stage can form strong hydrogen bonds with polar solvent molecules. And due to the polarity gap on both sides of DMEDA carbamic acid molecule, when the concentration of carbamic acid reaches a certain level, an ordered structure is likely to form in the solution, resulting in a significant increase in viscosity. Similar phenomena have been described in the literature [31,32].

Given the identical principal reactant DMEDA, the species distributions in aqueous and water-lean solutions become increasingly similar as saturation is approached. The carbamic acid, with its 1:1 stoichiometric ratio in the chemical reaction, emerges as the predominant product in the end. Since the extremely low concentration of free amine at this point, the k_l values of the aforementioned solutions are limited by the protonation rate of carbamate ions. As a result, they exhibit similar k_l and display a comparable downward trend. However, the difference in water content leads to the different amount of bicarbonate that eventually forms, which is why aqueous amine solutions are generally considered to have a larger saturation capacity, although the absorption rate is quite low at this time, and it is usually not economical to continue running until the absorbent tends to be saturated. However, given that EFH20 and EFH30 can still maintain robust mass transfer performance under certain loadings, moderately increasing water content to broaden the operational range of water-lean absorbents could be considered in

Table 4
CO_2 absorption kinetics parameters at 313.15 K under different CO_2 loadings

	α	K_G*	k_g*	k_l*	k_l^0	μ_l	ρ_l	$D_{CO2,l}$	$H_{CO2,l}$	E*
	mol/mol		mol·m^{-2}·s^{-1}·Pa^{-1}		m/s	mPa·s	kg/m^3	m^2/s	Pa·m^3·mol^{-1}	
DMEDA (aq.)	0	1.42E-06	3.21E-05	1.49E-06	5.86E-05	3.59	961.2	6.92E-10	3716.64	94.4
	0.1	1.29E-06	3.23E-05	1.34E-06	5.86E-05	3.60	976.8	6.90E-10	3716.64	84.8
	0.33	9.71E-07	3.22E-05	1.00E-06	5.86E-05	3.64	1011.4	6.84E-10	3716.64	63.5
	0.51	5.46E-07	3.18E-05	5.56E-07	5.84E-05	3.69	1038.1	6.77E-10	3716.64	35.3
	0.62	4.10E-07	3.23E-05	4.15E-07	5.83E-05	3.72	1053.9	6.72E-10	3716.64	26.4
	0.77	3.11E-07	3.21E-05	3.14E-07	5.81E-05	3.76	1076.8	6.67E-10	3716.64	20.0
	0.95	2.01E-07	3.18E-05	2.02E-07	5.80E-05	3.81	1104.1	6.60E-10	3716.64	13.0
EFH5	0	4.63E-06	3.22E-05	5.41E-06	1.04E-04	1.29	914.7	1.57E-09	1063.39	55.4
	0.25	4.14E-06	3.23E-05	4.74E-06	9.70E-05	1.46	932.6	1.42E-09	1063.39	52.0
	0.40	3.47E-06	3.24E-05	3.88E-06	9.04E-05	1.66	945.7	1.28E-09	1063.39	45.6
	0.45	2.65E-06	3.23E-05	2.88E-06	8.78E-05	1.75	948.5	1.23E-09	1063.39	34.9
	0.50	1.37E-06	3.23E-05	1.43E-06	8.34E-05	1.92	953.2	1.14E-09	1063.39	18.3
	0.55	5.69E-07	3.22E-05	5.80E-07	7.89E-05	2.12	956.4	1.05E-09	1063.39	7.81
	0.60	3.27E-07	3.21E-05	3.30E-07	7.46E-05	2.34	960.6	9.74E-10	1063.39	4.70
	0.85	2.16E-07	3.22E-05	2.17E-07	5.99E-05	3.47	977.1	7.11E-10	1063.39	3.86
EFH10	0	4.24E-06	3.18E-05	4.89E-06	8.96E-05	1.68	920.1	1.27E-09	1238.44	67.6
	0.36	3.39E-06	3.20E-05	3.79E-06	7.91E-05	2.10	949.7	1.06E-09	1238.44	59.3
	0.48	2.77E-06	3.18E-05	3.03E-06	7.43E-05	2.36	971.2	9.66E-10	1238.44	50.5
	0.58	1.91E-06	3.21E-05	2.04E-06	7.05E-05	2.59	971.2	8.97E-10	1238.44	35.7
	0.65	8.08E-07	3.21E-05	8.29E-07	6.56E-05	2.96	983.5	8.07E-10	1238.44	15.6
	0.75	3.10E-07	3.18E-05	3.13E-07	5.93E-05	3.54	983.5	7.00E-10	1238.44	6.53
	0.89	1.90E-07	3.21E-05	1.91E-07	5.04E-05	4.74	1001.6	5.54E-10	1238.44	4.70
EFH20	0	3.81E-06	3.23E-05	4.32E-06	7.88E-05	2.11	929.1	1.06E-09	1637.34	89.8
	0.22	3.31E-06	3.20E-05	3.69E-06	7.27E-05	2.45	956.2	9.40E-10	1637.34	83.0
	0.45	2.64E-06	3.20E-05	2.88E-06	6.52E-05	2.99	985.3	8.01E-10	1637.34	72.3
	0.55	2.22E-06	3.18E-05	2.38E-06	5.96E-05	3.51	994.3	7.04E-10	1637.34	65.4
	0.66	1.44E-06	3.20E-05	1.51E-06	5.32E-05	4.30	1002.9	5.98E-10	1637.34	46.4
	0.8	3.29E-07	3.20E-05	3.32E-07	4.45E-05	5.91	1015.2	4.64E-10	1637.34	12.2
	0.92	1.97E-07	3.21E-05	1.98E-07	3.96E-05	7.30	1025.7	3.92E-10	1637.34	8.17
EFH30	0	3.19E-06	3.21E-05	3.54E-06	7.08E-05	2.55	939.5	9.10E-10	2062.57	103
	0.21	2.52E-06	3.17E-05	2.74E-06	5.86E-05	3.60	974.9	6.90E-10	2062.57	96.3
	0.43	1.72E-06	3.22E-05	1.81E-06	5.05E-05	4.74	1011.4	5.54E-10	2062.57	74.1
	0.72	3.85E-07	3.20E-05	3.89E-07	4.18E-05	6.66	1032.8	4.22E-10	2062.57	19.2
	0.95	1.80E-07	3.18E-05	1.81E-07	3.20E-05	10.74	1063.8	2.88E-10	2062.57	11.7

* The values in this column are the arithmetic means of measurements taken at four different CO_2 partial pressures.

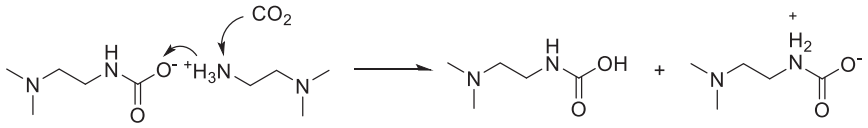

Fig. 10. Proton transfer of carbamate ion pairs

practical production, albeit at the cost of sacrificing some peak mass transfer efficiency.

4. Conclusion

Although the aqueous solution of linear terminal diamine DMEDA has advantages in CO_2 capacity and regeneration rate, the mass transfer coefficient of the liquid film is slightly lower than that of the traditional amine-based absorbent MEA (aq.). Replacing water in DMEDA(aq.) with aprotic polar solvent DMF inhibits chemical reactions to some extent. However, its low viscosity, excellent diffusion property, and high physical solubility of CO_2 greatly improve the physical mass transfer property of DMEDA absorbent, and promotes the entry and distribution of CO_2 into the liquid phase. This allows DMEDA water-lean absorbent to exhibit significantly high mass transfer property under low CO_2 loading. At 313.15 K, the k_l of fresh EFH5 can reach 3.6 times that of DMEDA(aq.).

The ^{13}C NMR spectrum shows significant differences in the transformation of species in EFH series and DMEDA(aq.). Although these absorbents have similar reaction kinetics due to the same main agent, the differences in the solvent environment lead to different forms of the products. In the early stage of the reaction, the carbamate is easily hydrolyzed in aqueous solution to form carbamic acid, but exists in the form of carbamate ion pairs in aprotic polar solvent. As the CO_2 loading increases, the free amine concentration decreases. In EFH5 and EFH10, the absorption rate is limited by the proton transfer rate of the carbamate ion pairs, hence the appearance of the inflection point in k_l. However, due to their superior physical mass transfer performance, these absorbents still retain a broader operational range. This advantage holds true even for EFH20 and EFH30, despite their relatively low organic solvent concentrations.

Therefore, in the development of amine-based water-lean absorbents, on the one hand, the physical mass transfer process in the early stage of the absorption should be enhanced, with viscosity and CO_2 solubility being the primary factors in solvent selection. On the other hand, the chemical reaction process in the middle stage of the reaction should be enhanced. Introducing a relatively more proton acceptors can ensure that the deprotonation process of carbamate zwitterion is not hindered, thereby broadening the operating range of the absorbent. Additionally, since the extensive formation of carbamic acid can lead to a sharp increase in viscosity, selecting a solvent with strong polarity can inhibit the hydrolysis of carbamate ion pairs through solvation effects, thereby delaying the formation of carbamate and helping to maintain the stability of the absorbent.

CRediT authorship contribution statement

Zhilv Chen: Writing – original draft, Methodology, Investigation, Formal analysis, Conceptualization. **Chaoming Jian:** Funding acquisition. **Chao Li:** Supervision, Methodology. **Tao Wang:** Writing – review & editing, Supervision, Resources. **Qinhui Wang:** Writing – review & editing, Supervision, Resources. **Mengxiang Fang:** Writing – review & editing, Supervision, Resources. **Fanpeng Meng:** Funding acquisition. **Wei Chen:** Funding acquisition. **Yongsheng An:** Funding acquisition. **Ximing Hu:** Formal analysis.

Declaration of competing interest

The authors declare that they have no known competing financial interests or personal relationships that could have appeared to influence the work reported in this paper.

Acknowledgments

This work is supported by National Key Research and Development Program of China (2023YFE0199300) , Pioneer R&D Program of Zhejiang Province -China (2022C03040), and the Fundamental Research Funds for the Central Universities (2022ZFJH004)

Appendix A. Supplementary data

Supplementary data to this article can be found online at https://doi.org/10.1016/j.cej.2025.164527.

Data availability

Data will be made available on request.

References

[1] M. Caplow, Kinetics of carbamate formation and breakdown, J. Am. Chem. Soc. (24) (1968) 6795, https://doi.org/10.1021/ja01026a041.
[2] Z. Chen, et al., Energy-efficient biphasic solvents for industrial carbon capture: role of physical solvents on CO(2) absorption and phase splitting, Environ. Sci. Technol. (18) (2022) 13305–13313, https://doi.org/10.1021/acs.est.2c05687.
[3] W. Jung, J. Lee, Kinetic modeling of polyamine-based water-lean solvents for CO2 capture: reverse temperature dependence of the overall mass transfer coefficient, Chem. Eng. Sci. (2022), https://doi.org/10.1016/j.ces.2021.117355.
[4] D. Barpaga, et al., Evaluation of a third generation single-component water-lean diamine solvent for post-combustion CO2 capture, ACS Sustain. Chem. Eng. 14 (2022) 4522–4528, https://doi.org/10.1021/acssuschemeng.1c08401.
[5] J. Liu, J. Qian, Y. He, Water-lean triethylenetetramine/N,N-diethylethanolamine/n-propanol biphasic solvents: phase-separation performance and mechanism for CO2 capture, Sep. Purif. Technol. (2022), https://doi.org/10.1016/j.seppur.2022.120740.
[6] Z. Chen, et al., Research on CO2 capture performance of DMEDA water-lean absorbents based on molecular dynamics, Sep. Purif. Technol. (2025), https://doi.org/10.1016/j.seppur.2024.128924.
[7] X.Y. Yu, et al., Mesoscopic structure facilitates rapid CO_2 transport and reactivity in CO_2 capture solvents, J. Phys. Chem. Lett. (19) (2018) 5765–5771, https://doi.org/10.1021/acs.jpclett.8b02231.
[8] R.R. Wanderley, et al., CO2 solubility and mass transfer in water-lean solvents, Chem. Eng. Sci. (2019) 403–416, https://doi.org/10.1016/j.ces.2019.03.052.
[9] F. Liu, et al., Mass transfer and kinetic measurement and modeling for CO2 absorption into aqueous EAE and water-lean EAE/NMP solvents, Chem. Eng. J. (2024), https://doi.org/10.1016/j.cej.2024.152346.
[10] C. Perinu, B. Arstad, K.-J. Jens, 13C NMR experiments and methods used to investigate amine-CO2-H2O systems, Energy Procedia (2013) 7310–7317, https://doi.org/10.1016/j.egypro.2013.06.669.
[11] H. Shi, et al., 13C NMR spectroscopy of a novel amine species in the DEAB–CO2–H2O system: VLE model, Ind. Eng. Chem. Res. (25) (2012) 8608–8615, https://doi.org/10.1021/ie300358c.
[12] Q. Yang, et al., A Carbon-13 NMR study of carbon dioxide absorption and desorption with aqueous amine solutions, Energy Procedia 1 (2009) 955–962, https://doi.org/10.1016/j.egypro.2009.01.127.
[13] W. Böttinger, M. Maiwald, H. Hasse, Online NMR spectroscopic study of species distribution in MEA–H_2O–CO_2 and DEA–H_2O–CO_2, Fluid Phase Equilib. (2) (2008) 131–143, https://doi.org/10.1016/j.fluid.2007.09.017.
[14] W. Böttinger, M. Maiwald, H. Hasse, Online NMR spectroscopic study of species distribution in MDEA-H2O-CO2 and MDEA-PIP-H2O-CO2, Ind. Eng. Chem. Res. 20 (2008) 7917–7926, https://doi.org/10.1021/ie800914m.
[15] C.K. Ahn, et al., Characterization of ammonia-based CO2 capture process using ion speciation, Int. J. Greenhouse Gas Control (6) (2011) 1606–1613, https://doi.org/10.1016/j.ijggc.2011.09.007.
[16] G. Lu, et al., Development of novel AMP-based absorbents for efficient CO2 capture with low energy consumption through modifying the electrostatic potential, Chem. Eng. J. (2023), https://doi.org/10.1016/j.cej.2023.145929.
[17] P.V. Kortunov, et al., In situ nuclear magnetic resonance mechanistic studies of carbon dioxide reactions with liquid amines in non-aqueous systems: evidence for the formation of carbamic acids and zwitterionic species, Energy Fuel 9 (2015) 5940–5966, https://doi.org/10.1021/acs.energyfuels.5b00985.
[18] Y. Yuan, G.T. Rochelle, CO2 absorption rate in semi-aqueous monoethanolamine, Chem. Eng. Sci. (2018) 56–66, https://doi.org/10.1016/j.ces.2018.02.026.
[19] Y. Xu, et al., CO2 absorption performance in advanced water-lean diamine solvents, Chem. Eng. J. (2021), https://doi.org/10.1016/j.cej.2021.131410.
[20] B. Yu, et al., Insights into the chemical mechanism for CO(2)(aq) and H(+) in aqueous diamine solutions - an experimental stopped-flow kinetic and (1)H/(13)C NMR study of aqueous solutions of N,N-dimethylethylenediamine for postcombustion CO(2) capture, Environ. Sci. Technol. (2018) 916–926, https://doi.org/10.1021/acs.est.7b05226, 2.
[21] B. Yu, et al., Characterisation and kinetic study of carbon dioxide absorption by an aqueous diamine solution, Appl. Energy (2017) 1308–1317, https://doi.org/10.1016/j.apenergy.2017.09.023.
[22] P. Paoletti, et al., Thermodynamic of protonation of amines. Values of log K, Δ H, and Δ S for the protonation of NN′-and NN-dimethylethylenediamine and NNN′ N′-tetramethylethylenediamine, J. Chem. Soc. a -Inorg. Phys. Theor. 2 (1971) 310, https://doi.org/10.1039/j19710000310.
[23] P.N. Sutar, P.D. Vaidya, E.Y. Kenig, Activated DEEA solutions for CO2 capture—a study of equilibrium and kinetic characteristics, Chem. Eng. Sci. (2013) 234–241, https://doi.org/10.1016/j.ces.2012.11.038.
[24] D. Nath, A. Henni, Solubility of carbon dioxide (CO2) in aqueous solution of 3-(dimethylamino)-1-propylamine (DMAPA), Fluid Phase Equilib. (2020), https://doi.org/10.1016/j.fluid.2020.112506.
[25] R.R. Wanderley, G.J.C. Ponce, H.K. Knuutila, Solubility and heat of absorption of CO2 into diisopropylamine and N,N-diethylethanolamine mixed with organic solvents, Energy Fuel 7 (2020) 8552–8561, https://doi.org/10.1021/acs.energyfuels.0c00880.
[26] M.A. Pacheco, Mass transfer, kinetics and rate-based modeling of reactive absorption, 1998.
[27] E.N. Fuller, P.D. Schettle, J.C. Giddings, A new method for prediction of binary gas-phase diffusion coeffecients, Ind. Eng. Chem. 5 (1966) 19, https://doi.org/10.1021/ie50677a007.
[28] S. Shen, et al., Kinetics of CO2 absorption into aqueous basic amino acid salt: potassium salt of lysine solution, Environ. Sci. Technol. (4) (2016) 2054–2063, https://doi.org/10.1021/acs.est.5b04515.
[29] G.F. Versteeg, W.P.M. Vanswaaij, Solubility and diffusivity of acid gases (CO2, N2O) in aqueous alkanolamine solutions, J. Chem. Eng. Data 1 (1988) 29–34, https://doi.org/10.1021/je00051a011.
[30] M. Laliberté, Model for calculating the viscosity of aqueous solutions, J. Chem. Eng. Data (2) (2007) 321–335, https://doi.org/10.1021/je0604075.
[31] L. Dougan, et al., Methanol-water solutions: a bi-percolating liquid mixture, J. Chem. Phys. (13) (2004) 6456–6462, https://doi.org/10.1063/1.1789951.
[32] Y. Zhong, G.L. Warren, S. Patel, Thermodynamic and structural properties of methanol-water solutions using nonadditive interaction models, J. Comput. Chem. 7 (2008) 1142–1152, https://doi.org/10.1002/jcc.20877.